ISSN 1674-1056
http://cpb.iphy.ac.cn
http://iopscience.iop.org/cpb
中国物理 B
Chinese Physics
中国物理
Chinese Physics B

Refractivity-from-clutter' based on local empirical refractivity model

Xiaofeng Zhao(赵小峰)

Citation: Chin. Phys. B . 2018, 27(12): 128401. **doi:** 10.1088/1674-1056/27/12/128401
Journal homepage: http://cpb.iphy.ac.cn; http://iopscience.iop.org/cpb

What follows is a list of articles you may be interested in

Perpendicularly oriented barium ferrite thin films with low microwave loss, prepared by pulsed laser deposition

Da-Ming Chen(陈大明), Yuan-Xun Li(李元勋), Li-Kun Han(韩莉坤), Chao Long(龙超), Huai-Wu Zhang(张怀武)
Chin. Phys. B . 2016, 25(6): 068403. **doi:** 10.1088/1674-1056/25/6/068403

Improved dichotomous search frequency offset estimator for burst-mode continuous phase modulation

Zhai Wen-Chao, Li Zan, Si Jiang-Bo, Bai Jun
Chin. Phys. B . 2015, 24(11): 118402. **doi:** 10.1088/1674-1056/24/11/118402

Study of a millimeter-wave squint indirect holographic algorithm suitable for imaging with large field-of-view

Gao Xiang, Li Chao, Fang Guang-You
Chin. Phys. B . 2014, 23(2): 028401. **doi:** 10.1088/1674-1056/23/2/028401

A novel four-legged loaded element thick-screen frequency selective surface with a stable performance

Tang Guang-Ming, Miao Jun-Gang, Dong Jin-Ming
Chin. Phys. B . 2012, 21(12): 128401. **doi:** 10.1088/1674-1056/21/12/128401

Photonic generation of arbitrary waveforms based on incoherent wavelength-to-time mapping

Dong Jian-Ji, Luo Bo-Wen, Yu Yuan, Zhang Xin-Liang
Chin. Phys. B . 2012, 21(6): 068401. **doi:** 10.1088/1674-1056/21/6/068401

"Refractivity-from-clutter" based on local empirical refractivity model*

Xiaofeng Zhao(赵小峰)†

College of Meteorology and Oceanography, National University of Defense Technology, Nanjing 211101, *China*

(Received 14 July 2018; revised manuscript received 23 September 2018; published online 25 November 2018)

Constructing sophisticated refractivity models is one of the key problems for the RFC (refractivity from clutter) technology. If prior knowledge of the local refractivity environment is available, more accurate parameterized model can be constructed from the statistical information, which in turn can be used to improve the quality of the local refractivity retrievals. The validity of this proposal was demonstrated by range-dependent refractivity profile inversions using the adjoint parabolic equation method to the Wallops'98 experimental data.

Keywords: refractivity-from-clutter, parabolic equation, adjoint method, empirical refractivity model

PACS: 84.40.–x, 07.07.Df **DOI:** 10.1088/1674-1056/27/12/128401

1. Introduction

Remote sensing of atmospheric refractivity from radar data is an effective complement for the traditional refractivity detection methods, such as radiosonde and rocketsonde.[1] The RFC technique contains three main aspects: (i) an accurate mapping between radar clutter data and refractivity, (ii) a reasonable cost function measuring the difference between the observed data and the replica field, and (iii) an efficient optimization method finding the optimal solution. Most of the previous publications focused on the third part and heuristic optimization algorithms, such as genetic algorithm,[2] support vector machine,[3] simulated annealing,[4] deep learning,[5] were used for the optimal searching.

In these inversions, a feasible measure for accuracy improvement is to reduce the nonlinearity of the problem as well as the number of the estimated parameters.[6–8] Although most commonly used refractivity parameterized models, such as log–linear evaporation duct model, segmented tri-linear model, and mixed duct model, can synoptically describe the real refraction environments,[9] these models are too simple to characterize some profiles in detail. Besides, the mathematical formulas of these models are nonlinear except for the log–linear evaporation duct model. Constructing more sophisticated refractivity models is one of the key points to improve the inversion accuracy.

This paper is an extension of the work completed by Zhao *et al.*,[8] where adjoint parabolic equation (PE) method has been proved to be efficient for range-dependent evaporation duct structures inversion in real-time. Here, the method is extended to general duct cases by using local a priori refractive information (supposed to be available) to formulate a more robust linear refractivity model, and the performance is validated by the Wallops'98 experimental data.

The remainder of this paper is organized as follows: Wallops'98 data, including radar data and refractivity data, are briefly introduced in Section 2. Section 3 presents the method for local empirical refractivity model construction based on the Wallops'98 refractivity data. The range-dependent refractivity retrievals are shown in Section 4. Finally, the conclusions are presented in Section 5.

2. Wallops'98 data

Detailed description about the Virginia Wallops'98 experiments and the data quality control can be found in Ref. [10] and Ref. [11]. A simple introduction about the data used in this paper is presented in this section.

2.1. Radar data

The radar signals were obtained using a Space Range Radar (SPANDAR) with an operational frequency of 2.84 GHz, a beam width of 0.39°, an elevation angle of 0°, an antenna height of 30.78 m, a range bin of 600 m, and vertical polarization. The antenna pattern was approximated as a $\sin(x)/x$ pattern. Four polar plots of clutter maps (corresponding to the time of 17:40 UT, 18:10 UT, 18:32 UT, and 19:00 UT April 02, 1998) from surface-based ducting events are shown in Fig. 1. The edges around radials 30° and 180°–200° are due to the coastline. It is clear that because of ducting propagation, many intensification patterns can be observed over the sight-of-horizon.

To mitigate the effects of point targets (including sea spikes), the radar data used in the inversions are median filtered across range (1.2 km, 3 samples) and azimuth (5°, 13 samples, *i.e.*, the increment of 0.4°). The filtered clutter data along the 150° radial (pink lines in Fig. 1) are shown in Fig. 2.

*Project supported by the National Natural Science Foundation of China (Grant Nos. 41775027 and 41405025).

†Corresponding author. E-mail: zxf_best@126.com

© 2018 Chinese Physical Society and IOP Publishing Ltd

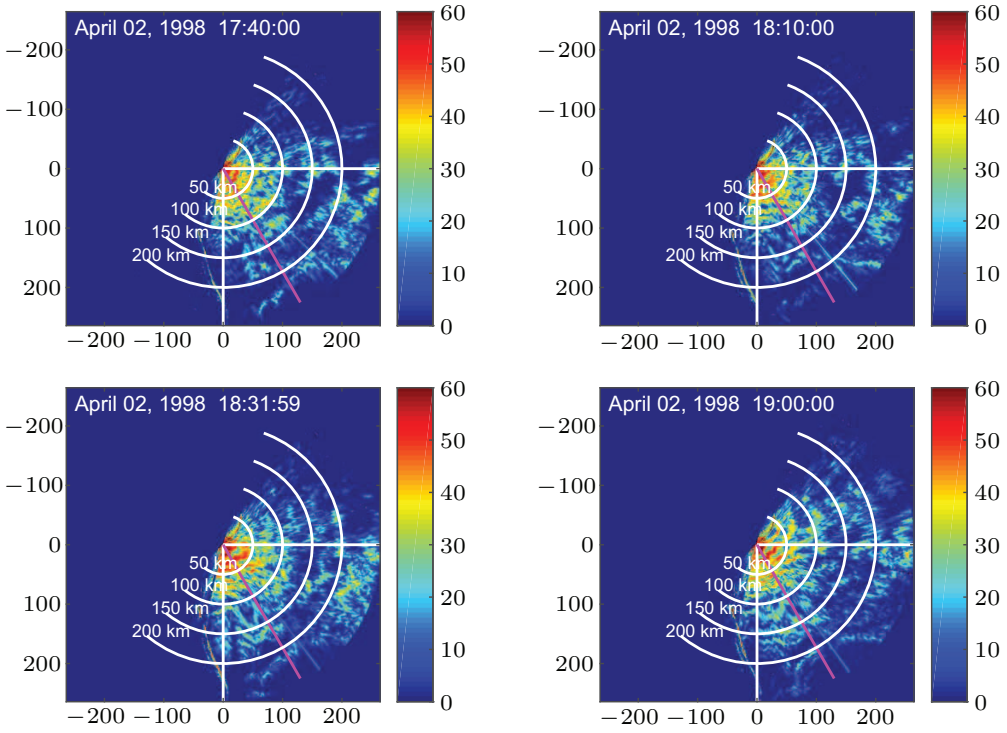


Fig. 1. (color online) Clutter echo (signal-to-noise ratio, measured in unit dB) from SPANDAR at the time of 17:40 UT, 18:10 UT, 18:32 UT, and 19:00 UT April 02, 1998.

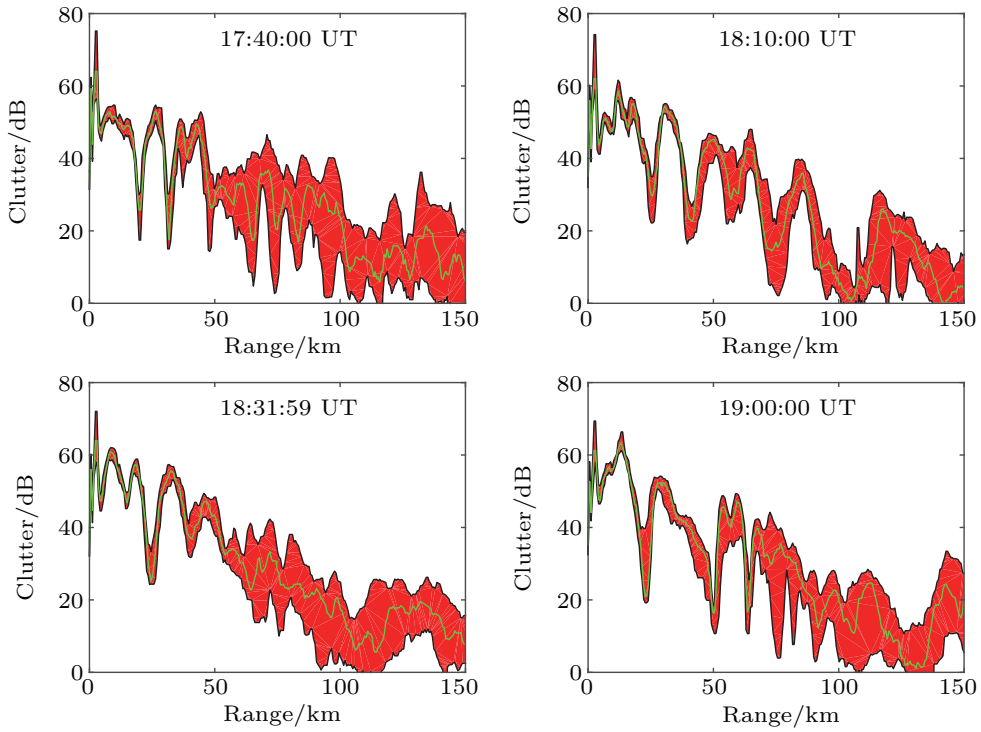


Fig. 2. (color online) Clutter returns as a function of range from 0 km to 150 km for different times. The red shaded area is the envelope of 13 returns in a 5°-interval, and the green line is the median.

2.2. Refractivity data

The refractive environments were recorded using an instrumented helicopter and a Chessie boat provided by the Applied Physics Laboratory of Johns Hopkins University. The helicopter flew a saw-tooth up-and-down pattern in and out along the 150° radial (pink lines in Fig. 1) from a point 4 km to 60 km due east of the SPANDAR. Contour plots of modified refractivity versus range and height corresponding to the measurements from time 13:47 UT to 21:52 UT April 02 1998 are shown in Fig. 3, where each subfigure has 32 refractivity profiles,[11] *i.e.*, the total number of profiles collected are 320.

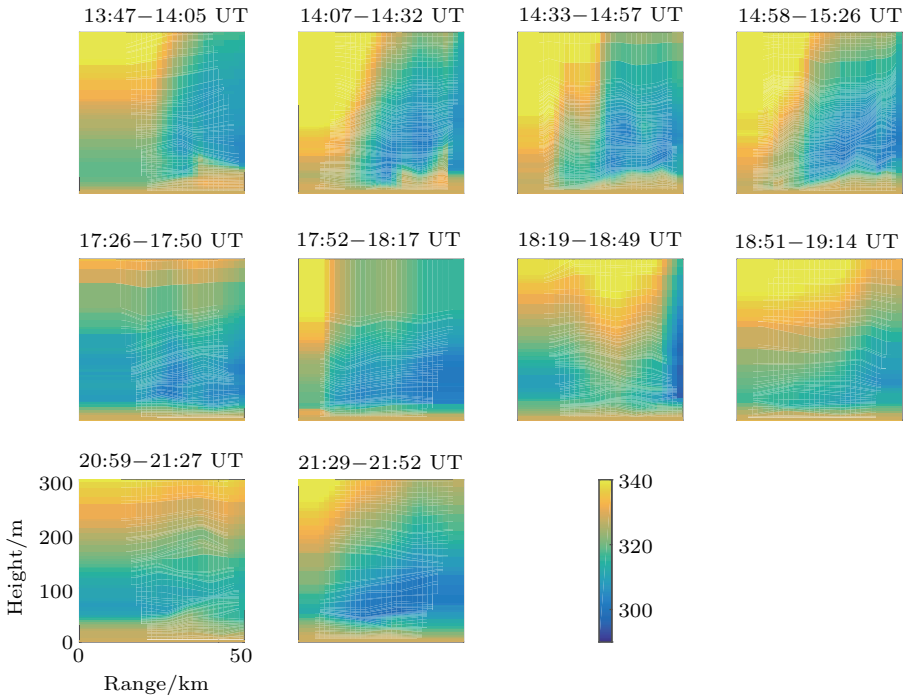


Fig. 3. (color online) Contour plots of modified refractivity (M units) versus range and height sequenced in time. All refractivity profiles have been normalized to the same value (333.8-M units) at sea level.

3. Local empirical refractivity model construction

For a particular region of interest, if reliable a priori refractivity information is available (*e.g.*, from historical measurements or outputs of numerical weather prediction models), more robust parameterized refractivity model can be constructed for this region by analyzing the principal characteristics of the provided prior information. The methods can be used for this purpose including empirical orthogonal function (EOF),[12] principal components analysis (PCA),[13] and Karhunen–Loeve (KL) transform,[14] *etc*.

Let there be K refractivity profiles $m_1(z),\ldots,m_K(z)$. It is understood that the height z is actually discrete with length N. Note the eigenvalues and eigenvectors of the covariance matrix of the data set as $\lambda_1,\ldots,\lambda_N$ and $\phi_1(z),\ldots\phi_N(z)$, where it is assumed that the eigenvalues and corresponding eigenvectors are arranged in the order $\lambda_1 > \lambda_2 \ldots > \lambda_N$. Then, any profile in the data set can be expressed as

$$m(z) = \bar{m}(z) + \sum_{i=1}^{N} c_i\phi_i(z) \approx \bar{m}(z) + \sum_{i=1}^{N_T} c_i\phi_i(z), \qquad (1)$$

where $\bar{m}(z)$ is the mean profile and c_i are the coefficients that need to be determined. It is usually pointless and unnecessary to estimate the whole coefficients, especially when the number N is too large. For a practical problem, only the N_{T} ($N_{\mathrm{T}} \leq N$) principal components are used to balance the accuracy and the complexity. The number of N_{T} can be determined by the weight of magnitude of the eigenvalues.

For the inversion purpose, the helicopter-based refractivity profiles were used as the basic prior information to construct the local linear empirical refractivity model. Make perturbations to each profile at every sampling height in Fig. 3 with zero mean Gaussian noise of variance (3 M-units)^2 and smooth the perturbed profile by a 4-th-order polynomial fit, seeing Fig. 4(a) where the black line is the helicopter-based profile at range 0 km during 13:47–14:05 UT, the green line is the perturbed profile, and the blue line is the polynomial fitted profile. Repeating this process 100 times for each profile, then we obtained 32320 refractivity profiles (32000 polynomial fitted realizations plus 320 original observed profiles) which provided more possibilities of the real refractive environments and were used as the a priori refractivity information in this paper. The first 10 eigenvalues of all these 32320 refractivity profiles are given in Fig. 4(b), where the weight of the summation of first 4 eigenvalues is over 90%. Thus, it is reasonable to use the first 4 corresponding eigenvectors shown in Fig. 4(c) as the basis to approximate each refractivity profile, *i.e.*, $N_{\mathrm{T}} = 4$.

The refractivity fields in Fig. 3 show substantial range dependency, which indicates that a range-dependent model is needed for inversion purpose. Referring to the work completed by Gerstoft *et al.*,[11] range dependency can be described by 6 profiles at the range of 0 km, 12 km, 24 km, 36 km, 48 km, and 60 km. The profiles in between are linearly interpolated. Then the total estimated coefficients for refractivity profiles are 24 (4 coefficients for each profile multiply 6 profiles).

Compared with the traditional parameterized refractivity models (segmented tri-linear model, mixed duct model, *etc*.), the primary advantage of the local empirical model is that it is completely linear, which reduces the nonlinearity of the adjoint RFC problem and simplifies the corresponding computations, although it just can be used for local inversion purposes.

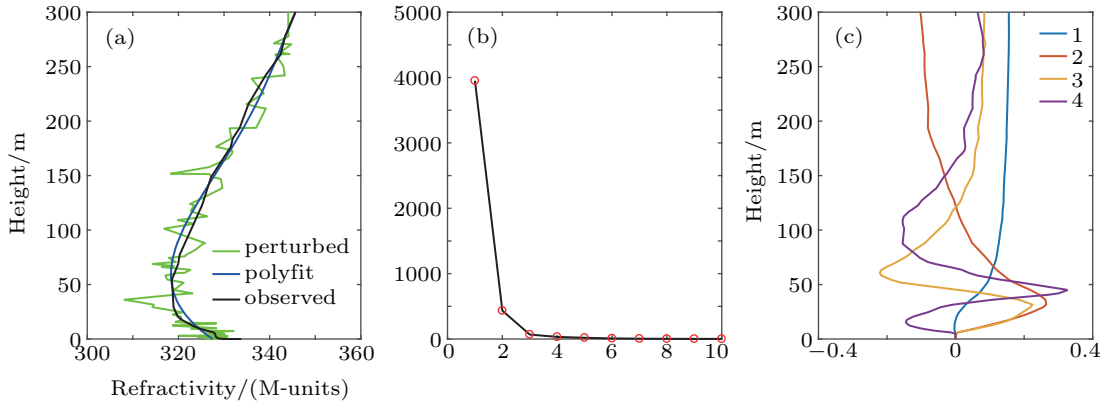


Fig. 4. (color online) The statistical information of a priori refractivity profiles, (a) the refractivity profiles, (b) the first 10 eigenvalue, and (c) the first 4 eigenvector.

4. Inversion results

The adjoint PE method for range-dependent refractivity profiles inversion was described in Ref. [8]. More detailed adjoint PE derivation can refer to Ref. [6]. How to make use of the a priori refractive information for the inversions is introduced in this Section.

The relationship between radar clutter power and refractivity parameters can be formulated as[8]

$$P_{\mathrm{r}}(x,\boldsymbol{m},\sigma)=40\log_{10}|u(x,z_{\mathrm{eff}},\boldsymbol{m})|-10\log_{10}(x)+\sigma, \quad (2)$$

where x is the range and z_{eff} is the effective scattering height and usually approximates 1 m above the ocean surface.[9] Term σ is a normalization constant determined by radar system parameters and the mean sea radar cross section (RCS) averaged over the range. Knowing an accurate value of the averaged RCS is difficult, especially at low grazing angles. Therefore, term σ can be treated as an unknown parameter. Term u is the complex electric field that can be computed from a split-step Fourier PE method.[15]

The mismatch between the predictions and the observations can be quantified by a least-squares form cost function. With the background (or a priori) information, the cost function can be modified as

$$J=\frac{1}{2}\left[P_{\mathrm{r}}-P_{\mathrm{r}}^{\mathrm{obs}}\right]^{\mathrm{T}}\boldsymbol{O}^{-1}\left[P_{\mathrm{r}}-P_{\mathrm{r}}^{\mathrm{obs}}\right]+\sum_{i=1}^{K}\frac{1}{2}\left[\boldsymbol{m}_i-\boldsymbol{m}^{\mathrm{b}}\right]^{\mathrm{T}}\boldsymbol{B}^{-1}\left[\boldsymbol{m}_i-\boldsymbol{m}^{\mathrm{b}}\right], \quad (3)$$

where P_{r} is the clutter predictions computed by Eq. (2) and $P_{\mathrm{r}}^{\mathrm{obs}}$ is the clutter observations. $\boldsymbol{m}_i=[c_1,\ldots,c_{N_{\mathrm{T}}}]^{\mathrm{T}}$ is the coefficient vector that needs to be estimated, i is the range index of the refractivity profiles. $\boldsymbol{m}^{\mathrm{b}}$ is the background field for coefficient $\boldsymbol{m}_i$. The matrices $\boldsymbol{O}$ and $\boldsymbol{B}$ are the clutter observation and refractive background error covariance, respectively.

For the problem in this paper, the number of the total estimated parameters is 25, *i.e.*, $N_{\mathrm{T}}=4$ times 6 profiles at the ranges of 0 km, 12 km, 24 km, 36 km, 48 km, and 60 km plus the nuisance parameter σ. The matrix $\boldsymbol{O}$ was set with elements of the variance of the clutter noise, and matrix $\boldsymbol{B}$ was set diagonal with elements of the first four eigenvalues in Fig. 4(b). The optimization process was performed by a quasi-Newton method,[16] and the maximum iteration number was set 400 to terminate the algorithm. With the computation source of a ThinkPad T440 with i7-4700MQ CPU and 8-GB RAM, all the four inversion examples can be finished within 30 seconds. The inversion results and comparisons with the observed data are given in Fig. 5, where the radar clutter profiles (from top to bottom corresponds to the time of 17:40 UT, 18:10 UT, 18:32 UT, and 19:00 UT) are marked in black, the inverted refractivity profiles and inverted-based clutter profiles are marked in red, and the helicopter refractivity profiles (from top to bottom corresponds to the time bin of 17:26 UT–17:50 UT, 17:52 UT–18:17 UT, 18:19 UT–18:49 UT, and 18:51 UT–19:14 UT) and helicopter-based clutter profiles are marked in blue.

From the left column of Fig. 5, it is clear seen that the inverted refractivity profiles can synoptically reflect the duct structures and their range-varying characteristics observed by the helicopter, but these two kinds of profiles do not fully match well with each other. The reason for this phenomenon is that: 1) each group of helicopter-based refractivity profiles was observed within a time range about 25 minutes, but the inverted profiles just reflect the instantaneous refractivity information corresponding to each clutter measurement. When the refractive environment varies with time, the 25 minutes bin observations definitely introduce errors. 2) The helicopter flew in a saw-tooth up-and-down pattern and the refractivity near the sea surface was not available by the helicopter, which can also cause electromagnetic (EM) prediction errors.

In the right column of Fig. 5, the patterns of the inverted-based clutter profiles agree well with that of the SPANDAR clutter observations, while the clutter patterns computed from the helicopter-based refractivity profiles deviate far from the observations. This is because for the tropospheric EM propagation problem, the propagation characteristics are mainly determined by the refractive conditions. Small differences in the refractivity structure can cause large errors in the EM prop-

agation simulations. This also demonstrates why it needs to acquire accurate refractive information in real time. From the clutter comparisons, it can infer that the inverted refractivity profiles describe the real refractive environment better than that of the helicopter-based profiles observed during about 25 minutes. All the four pairs of inversion results show similar conclusions, which indicate the validity and stability of the proposed method.

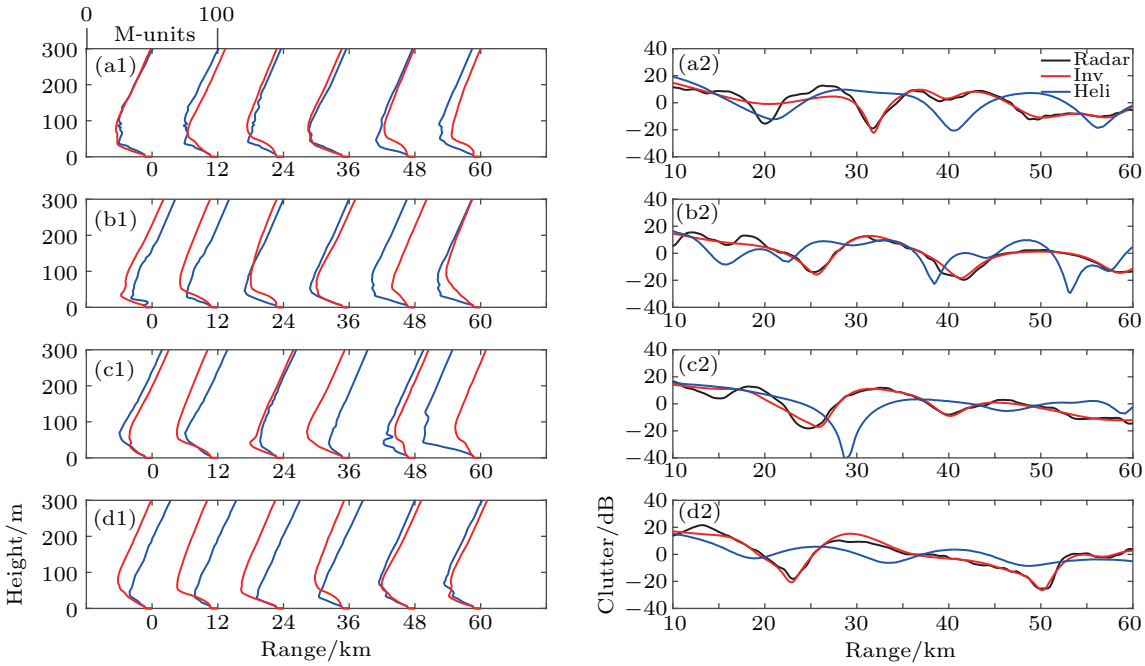


Fig. 5. (color online) The inversion results and comparisons with the observed data, where the left column compares the inverted refractivity profiles (red) with the helicopter observed profiles (blue), and the right column compares the inverted clutter strength (red) and helicopter-based profiles (blue) with the radar clutter strength (black). To eliminate the influence of the uncertainty value of σ on the helicopter-based clutter strength, all the clutter data were modified by subtracting each mean value.

5. Conclusions

This paper addresses the problem of how to use the a priori refractive information to formulate a more robust linear refractivity model for real-time RFC inversions. The validity of this method was demonstrated by range-dependent refractivity profile inversions using Wallops'98 experimental data. Although the results show promise, the proposed method is just aimed at local refractivity inversion purpose. Only 320 available helicopter-based refractivity profiles were used as the basis to construct the prior information. Future work is required to evaluate the performance of the method with more real data.

Acknowledgment

The Wallops'98 experimental data used in this paper were acquired from http://www.mpl.ucsd.edu/people/pgerstoft/.

References

[1] Zhang J P, Zhang Y S, Wu Z S, Zhang Y S and Hu R X 2015 *Acta Phys. Sin.* **64** 124101 (in Chinese)

[2] Penton S E and Hackett E E 2018 *Radio Sci.* **53** 804

[3] Douvenot R, Fabbro V, Gerstoft P, Bourlier C and Saillard J 2008 *Radio Sci.* **43** RS6005

[4] Zhao X F, Huang S X, Xiang J and Shi W L 2011 *Chin. Phys. B* **20** 099201

[5] Zhu X, Li J, Zhu M, Jiang Z and Li Y 2018 *IEEE Geosci. Remote S.* **15** 1307

[6] Zhao X F and Huang S X 2012 *J. Atmos. Sci.* **69** 2808

[7] Zhao X F and Huang S X 2014 *J. Atmos. Oceanic Technol.* **31** 1250

[8] Zhao X F, Yardim C, Wang D X and Howe B M 2017 *J. Atmos. Oceanic Technol.* **34** 1113

[9] Karimian A, Yardim C, Gerstoft P, HodgkissWS and Barrios A E 2011 *Radio Sci.* **46** RS6013

[10] Rogers L T, Hattan C P and Stapleton J K 2000 *Radio Sci.* **35** 955

[11] Gerstoft P, Rogers L T, Krolik J L and Hodgkiss W S 2003 *Radio Sci.* **38** 8053

[12] Liu X, Huang W and Gill E W 2017 *IEEE Geosci. Remote S.* **14** 1740

[13] Xie J, Chen W, Zhang D, Zu S and Chen Y 2017 *IEEE Geosci. Remote S.* **14** 1213

[14] Li J, Innanen K A, Tao G 2017 *Geophysics* **82** D265

[15] Kuttler J R and Dockery G D 1991 *Radio Sci.* **26** 381

[16] Zhu C, Byrd R H, Lu P and Nocedal J 1997 *ACM Trans. Math. Softw.* **23** 550